Powder processing of ductile-phase-toughened Nb–Nb_3Al *in situ* composites

L. Murugesh, K. T. Venkateswara Rao and R. O. Ritchie

Department of Materials Science and Mineral Engineering, University of California, Berkeley, CA 94720 (USA)

(Received November 19, 1993)

Abstract

Model high temperature Nb–Nb_3Al *in-situ* intermetallic matrix composites have been successfully fabricated using powder metallurgy and arc-melting techniques. Vacuum hot pressing of elemental Nb and Al powders, mixed in the ratio Nb–6wt.%Al and synthesized at 1200 °C, yielded a dual-phase microstructure consisting of equiaxed islands of ductile Nb particles in a brittle Nb_3Al matrix. Subsequent thermal treatment at 1800 °C for 24 h resulted in an alternative composite microstructure with the Nb present in a lamellar morphology following a peritectic transformation, similar to structures obtained via arc-melting and thermal treatment procedures. The precipitation of ductile Nb phase following thermal aging was found to nucleate heterogenously at grain boundaries and to progress along specific growth directions, resulting in a uniform and fine distribution of filamentary Nb within the Nb_3Al matrix. Both equiaxed and lamellar Nb–Nb_3Al composite microstructures show improved fracture toughness of about 6 MPa $m^{1/2}$ compared with unreinforced Nb_3Al (about 1 MPa $m^{1/2}$), principally because of crack bridging and crack renucleation effects induced by the presence of the ductile Nb phase.

1. Introduction

Niobium-aluminide-based intermetallic alloys have recently been the subject of much research aimed at designing new structural materials for use at high temperatures in advanced aerospace propulsion systems [1–3]. Specifically, the goal is to develop materials for structural applications above service temperatures of 1100 °C, and as high as 1650 °C, beyond the usable range of directionally solidified single-crystal and oxide-dispersion-strengthened nickel-based superalloys, at present used in gas turbine engines. Since, the efficiency and total thrust of a jet engine are a direct function of the peak temperature of the working fluid and current operating limits are set by thermal constraints on materials, the next generation of high performance engines will require markedly stiffer materials operating at higher stresses and much higher temperatures. Materials systems for these applications include other ordered intermetallics, and ceramics and their composites, all of which suffer from problems of low ductility and toughness.

Niobium aluminide alloys are preferred over many refractory-metal compounds because of their lower density. Among the various Nb aluminides, namely Nb_3Al, Nb_2Al and $NbAl_3$ (Fig. 1), the higher melting temperature and better creep resistance of Nb_3Al makes it the most promising [1, 2]. Like most intermetallics, Nb_3Al has a low symmetry, complex (A15) crystal structure (Fig. 2), with a melting point of 2060 °C and a density of 7.29 g cm^{-3}. However, the complex structure is simultaneously responsible for its high temperature strength and extreme susceptibility to brittle fracture at room temperature. Recent efforts have therefore been aimed at enhancing the ambient temperature ductility and fracture properties of Nb_3Al alloys.

One approach to improving the toughness of brittle intermetallics such as Nb_3Al is to fabricate an Nb_3Al composite by incorporating a refractory ductile metal phase in the microstructure; the principle here is to induce ductile-phase toughening, primarily by impeding crack advance via ductile-ligament bridging in the crack wake [4]. Such composites can be processed either by utilizing *in-situ* phase transformations in the alloy system through arc melting and thermomechanical treatments [5, 6], or by artificially hybridizing the microstructure with ductile phases [7–10]. As shown in Fig. 1, Nb_3Al is formed by a peritectic reaction at 2060 °C [11] with uniquely sloping phase boundaries such that the Nb-rich solid solution (Nb_{ss}) overlaps the intermetallic at high temperatures; this aspect of the phase formation provides a mechanism for the *in-situ* precipitation of duplex microstructures of Nb_3Al composites with excess Nb_{ss} as the ductile reinforcement phase. Previous studies have shown this to be a sluggish

0921-5093/94/$7.00
SSDI 0921-5093(94)09562-B

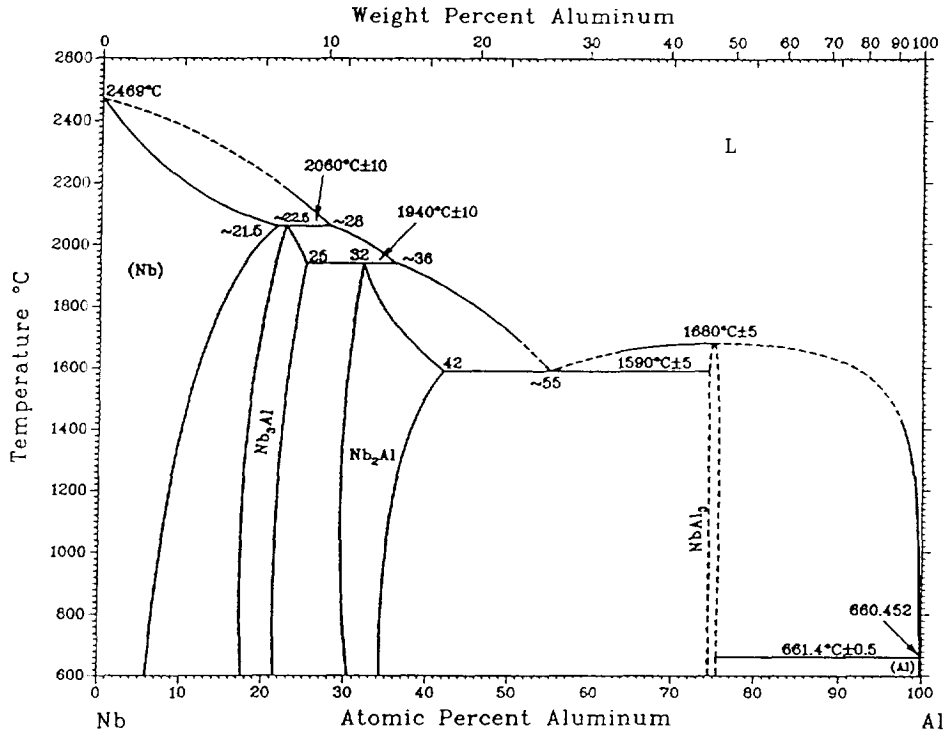

Fig. 1. The Nb–Al binary phase diagram.

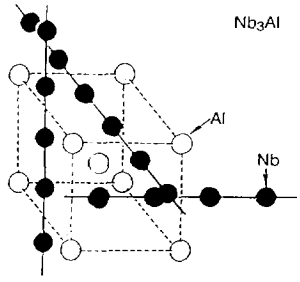

Fig. 2. The A15 crystal structure of Nb_3Al intermetallic compound.

transformation, such that Nb_{ss} can be retained at room temperature with only a moderate degree of undercooling [11–13]; further thermal treatment is necessary to precipitate the ordered second phase. The precipitation is reported to occur through a massive transformation, resulting in a highly uniform and fine distribution of a filamentary Nb within a non-contiguous Nb_3Al matrix [11].

The purpose of this paper is to examine alternative processing routes, specifically based on powder metallurgy (P/M) and reactive sintering techniques, for fabricating dual-phase Nb–Nb_3Al composite microstructures with improved ambient-temperature toughness induced by ductile-phase-bridging mechanisms; the microstructures and properties are compared with those obtained using arc-melting techniques.

2. Experimental procedures

2.1. Powder processing of Nb–Nb_3Al microstructures

Commercially pure Nb powder (1–10 μm size) was obtained from Cerac, Inc., Milwaukee, WI; atomized Al powder (about 3 μm size) was obtained from Valimet, Inc., Stockton, CA. The powders were mixed in the ratio of Nb–6wt.%Al (Nb–18at.%Al), prior to ball milling for 20 min at room temperature. The mixed powder was then synthesized by heating *in vacuo* to 1400 °C at a rate of 20 °C min^{-1} to initiate the reaction

$$Nb + 3Al \rightarrow Nb_3Al$$

The powders were held at 1400 °C for 1 h and stored in an argon atmosphere to prevent oxidation; the sintering sequence was repeated to ensure complete synthesis of Nb_3Al from the elemental Nb and Al powders.

Subsequently the synthesized Nb_3Al powder was compacted using a graphite die of 38 mm diameter and hot pressed *in vacuo* by simultaneously increasing the pressure and temperature to 36 MPa and 1650 °C respectively, holding for 10 min and then cooling to room temperature. Several samples were fabricated in a single operation by separating the powders by graphite spacers, coated with a boron nitride lubricant to prevent welding between graphite and the synthesized Nb–Al powder. The resulting samples obtained

from hot pressing about 25 g of synthesized powder were disks, about 38 mm in diameter and about 2.5 mm thick, which were readily amenable for fracture mechanics testing.

2.2. Arc melting of Nb–Nb_3Al microstructures

Alloys were also prepared by arc melting rods of Nb and Al in a water-cooled copper hearth under an inert atmosphere in the ratio of Nb–7wt.%Al (Nb–20at.%Al). The higher Al content was necessary to compensate for Al vaporization losses during processing; the final composition was determined to be Nb–5wt.%Al from energy-dispersive X-ray spectroscopy (EDS) measurements. However, arc melting results in a sample in the form of a button which is difficult to machine in the final form of a mechanical test specimen for fracture and fatigue testing.

2.3. Thermal treatment of Nb–Nb_3Al microstructures

To develop a composite microstructure with a lamellar Nb morphology, vacuum hot-pressed (P/M processed) Nb–Nb_3Al compacts were thermally aged for 1, 4 and 24 h, at 1800 °C in an inert environment, and cooled at 15 °C min^{-1} to room temperature. The samples were additionally annealed at 1450 °C for 24 h to reduce internal stresses and to consolidate the lamellar microstructure. Similarly, the Nb lamellae in arc-melted samples were slightly coarsened by thermal exposures at 1450 °C for up to 24 h.

2.4. Preparation of monolithic Nb_3Al

Pure (unreinforced) Nb_3Al was prepared by mixing and arc melting Nb and Al rods in the ratio Nb–9wt.%Al (Nb–25at.%Al); volatilization after flipping and remelting the sample four times resulted in samples of composition Nb–7wt.%Al, assessed using EDS methods. The samples contained several cracks from rapid quenching in the water-cooled hearth of the furnace; these were later ball milled for 2 h to fine Nb_3Al powder, before vaccum hot pressing at 1500 °C for 15 min at a pressure of 36 MPa. The final samples were in the form of discs, about 38 mm in diameter and about 2.5 mm thick.

2.5. Microstructural characterization and fracture testing

Sections of all samples were metallographically polished, etched using a solution of 10 ml of HNO_3, 10 ml of HF and 30 ml of lactic acid, and examined using optical and scanning electron microscopy. Specimens for transmission electron microscopy (TEM) were prepared by ion milling thin disks, 3 mm in diameter, that were thinned by prior mechanical grinding and polishing. X-ray diffraction (XRD) studies were performed on all alloys to identify the phases present in the different microstructures; the final compositions were estimated using EDS.

The fracture toughnesses K_{Ic} for Nb_3Al, Nb and the various Nb–Nb_3Al composites were evaluated by monotonically loading fatigue-precracked disk-shaped compact tension specimens 25 mm wide and 2.5 mm thick to failure, according to procedures detailed in *ASTM Standard E-399-90* [14]. Additional tests on selected microstructures were performed using the Vickers diamond indenter at loads between 10 and 15 kg to initiate cracking. The flexure properties of the materials were determined using beams 4 mm square and 12 mm long loaded in four-point bending.

3. Results and discussion

3.1. Microstructures

3.1.1. Powder processed Nb–Nb_3Al

The composite Nb–Nb_3Al microstructure obtained through P/M processing *i.e.* by vacuum hot pressing the synthesized Nb–6wt.%Al powders at 1650 °C, is shown in Fig. 3(a). The duplex microstructure consists predominantly of approximately 5 μm-sized equiaxed islands of Nb_{ss} (light phase) dispersed as a secondary phase in an Nb_3Al matrix, as expected from the Nb–Al phase diagram (Fig. 1); the volume fraction of the ductile Nb_{ss} phase is estimated to be about 40 vol.%.

The corresponding XRD pattern, shown in Fig. 4(a), also reveals intensity peaks characteristic of Nb_3Al and Nb. Although several peaks of Nb, Nb_3Al and Nb_2Al phases can overlap, the presence of Nb and Nb_3Al can be unambiguously identified from the diffracted intensities of Nb_3Al (320) ($2\theta = 64.7°$) and Nb (112) ($2\theta = 69.8°$). However, similar to previous studies [11, 12], it may be noted that the Nb_3Al peaks are displaced slightly to the left of actual stoichiometry (Nb–25at.%Al), while the Nb peaks are shifted to the right of the intensity peaks expected for pure Nb. This indicates the presence of Nb in the form of Nb_{ss} phase with a slightly reduced lattice parameter ($a_{Nb_{ss}} = 3.275$ Å *vs.* 3.305 Å for pure Nb) accounting for the peak shift toward higher 2θ values. Similarly, Nb_3Al has a smaller lattice parameter, presumably owing to a lower Al content than expected from stoichiometry. EDS analyses also confirm these notions; the Nb_3Al matrix is found to be Nb–23at.%Al with the secondary Nb_{ss} phase containing about 12.5 at.% Al, close to the solid solubility limit of Al in Nb at the elevated temperature.

Small amounts of elemental Al and Nb were also present owing to incomplete synthesis of the Nb and Al powders; these are seen as minute dark and light particles in Fig. 3(a). Minor traces of Nb_2Al and $NbAl_3$

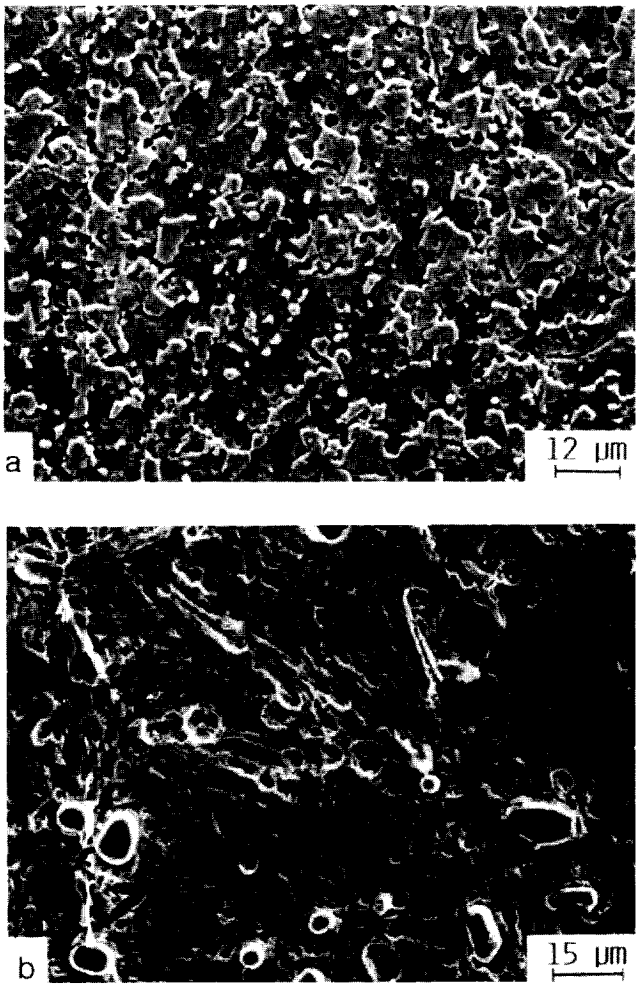

Fig. 3. Scanning electron micrographs of the microstructural features in the Nb–6wt.%Al alloy after (a) vacuum hot pressing the synthesized Nb–Al powder at 1650 °C and (b) following 24 h thermal treatment at 1800 °C. Note the equiaxed Nb morphology in (a) prior to the peritectic transformation compared with the lamellar structure in (b).

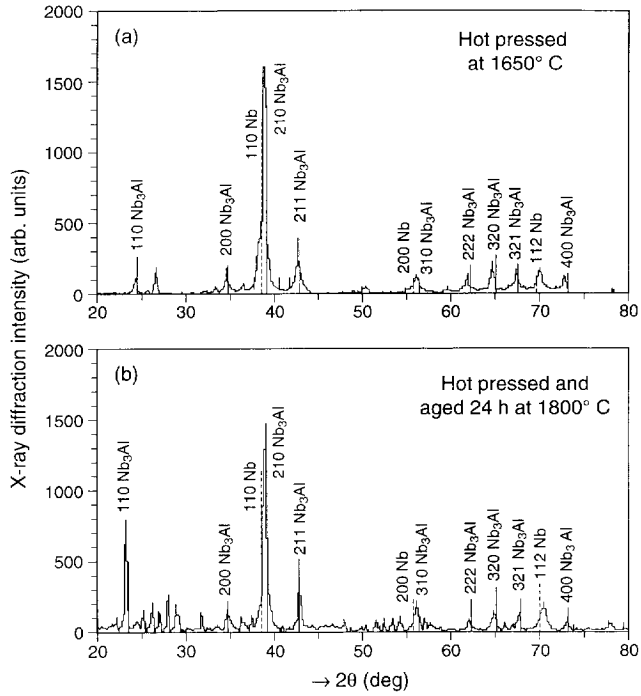

Fig. 4. XRD patterns of the Nb–6wt.%Al alloy showing the characteristic peaks for the Nb in solid solution and Nb_3Al phase after (a) vacuum hot pressing the reactively synthesized Nb–6wt.%Al powder at 1650 °C and (b) following 24 h thermal treatment at 1800 °C. The full and broken vertical lines correspond to the expected peaks at stoichiometry for the Nb_3Al and Nb phases respectively.

were also present because of the localized nature of the synthesis. Although the hot pressing of synthesized Nb_3Al powder resulted in sufficiently dense samples, some porosity is still apparent (Fig. 3a); the densification, however, is far greater than that achieved through simple hot pressing of elemental (unsynthesized) Nb and Al powders [15].

3.1.2. *Influence of thermal treatment*

A typical microstructure, obtained after heat treating the as hot-pressed (equiaxed) Nb–6wt.%(Nb–Nb_3Al) alloy at 1800 °C for 24 h, is illustrated in Fig. 3(b); the corresponding XRD pattern is shown in Fig. 4(b). Both Nb_3Al and Nb phases are clearly evident although the ductile-Nb-phase morphology is clearly altered owing to the peritectic transformation; the structure now contains lamellae of Nb_3Al with a stringy Nb_{ss} phase between them. The Nb_{ss} phase is rather fine, on the order of a few microns in thickness, and distributed uniformly throughout the matrix. At lower aging times of 1 and 4 h, however, the duplex Nb–Nb_3Al structure is not fully developed and the alloy retains Nb_{ss} with fine substructural features indicative of the early stages of transformation.

The decomposition of $Nb_{ss} \rightarrow Nb + Nb_3Al$ through the peritectic reaction is seen to nucleate heterogeneously at prior Nb_{ss} grain boundaries and to extend into the grain interior (Figs. 5 and 6). Analysis of TEM selected-area diffraction patterns reveals that the lamellar growth of Nb–Nb_3Al colonies occurs along the $Nb_{ss}\langle 110\rangle$ and $Nb_3Al\langle 211\rangle$ direction (see also ref. 16), although previous studies have suggested a different growth direction for Nb_3Al [17]. The lamellae then fuse into small elongated grains with a 5–8° misorientation between them (Fig. 6(c)). A high density of dislocations and bend contours is observed within the Nb_{ss} and the ordered Nb_3Al phases respectively (Figs. 6(b) and 6(c)); this is presumably related to the strains associated with the peritectic transformation and mismatch in thermal expansion properties. In fact,

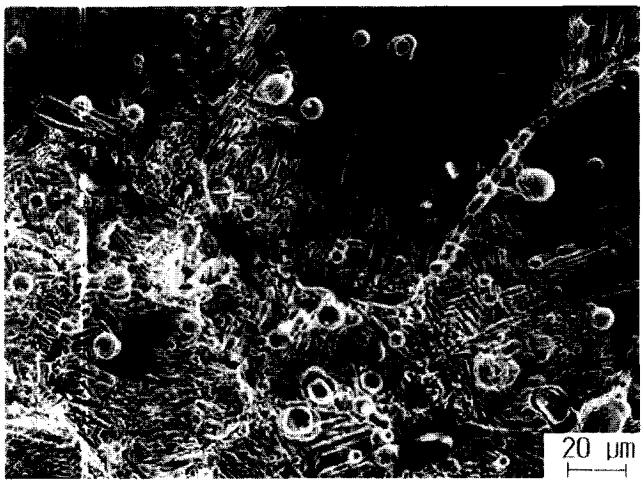

Fig. 5. Scanning electron micrograph of the hot-pressed Nb–6wt.% alloy aged for 24 h at 1800 °C, showing evidence of nucleation of lamellar Nb_3Al at grain boundaries and growth into the Nb_{ss} matrix.

previous work [18, 19] on A15 compounds has shown that, since Nb_3Al has a substantial mismatch with the parent Nb_{ss}, the initial precipitates are likely to be under considerable strain. Alternatively, compressive and tensile strains can be set up from lattice movement associated with the different diffusivities of Nb and Al. Such internal strain may, however, be relieved partially by the preferential nucleation of the Nb_3Al along grain boundaries and/or matrix dislocations.

3.1.3. Arc-melted Nb–Nb_3Al

The microstructure of the arc-melted Nb–7wt.%Al rods (Fig. 7(a)) also reveals the presence of Nb_{ss} dendrites at room temperature. The retention of the Nb solid solution at room temperature can be explained by following the solidification sequence of a molten Nb–5wt.%Al (Nb–15at.%Al) alloy (after accounting for volatilization losses of about 2 wt.% Al during arc melting). As the alloy cools, the first phase to appear is the Nb solid solution with a composition Nb–5at.%Al. The Nb_{ss} grows dendritically with successive layers solidifying at compositions determined by the local temperature and the Nb_{ss} solidus. As the remaining liquid becomes rich in Al, the Nb_3Al phase can precipitate surrounding Nb_{ss} dendrites. Incomplete diffusion in the Nb_{ss} solid and/or across the Nb_3Al phase (owing to fast cooling rates achieved in the water-cooled copper hearth) effectively prevents the peritectic reaction. Dendritic solidification, with no diffusion in the solid, can lead to the formation of small amounts of Nb_2Al and $NbAl_3$ around the Nb_{ss} dendrites; this is revealed as preferential etching due to the entrapped phases between the dendrites (Fig. 7(a)).

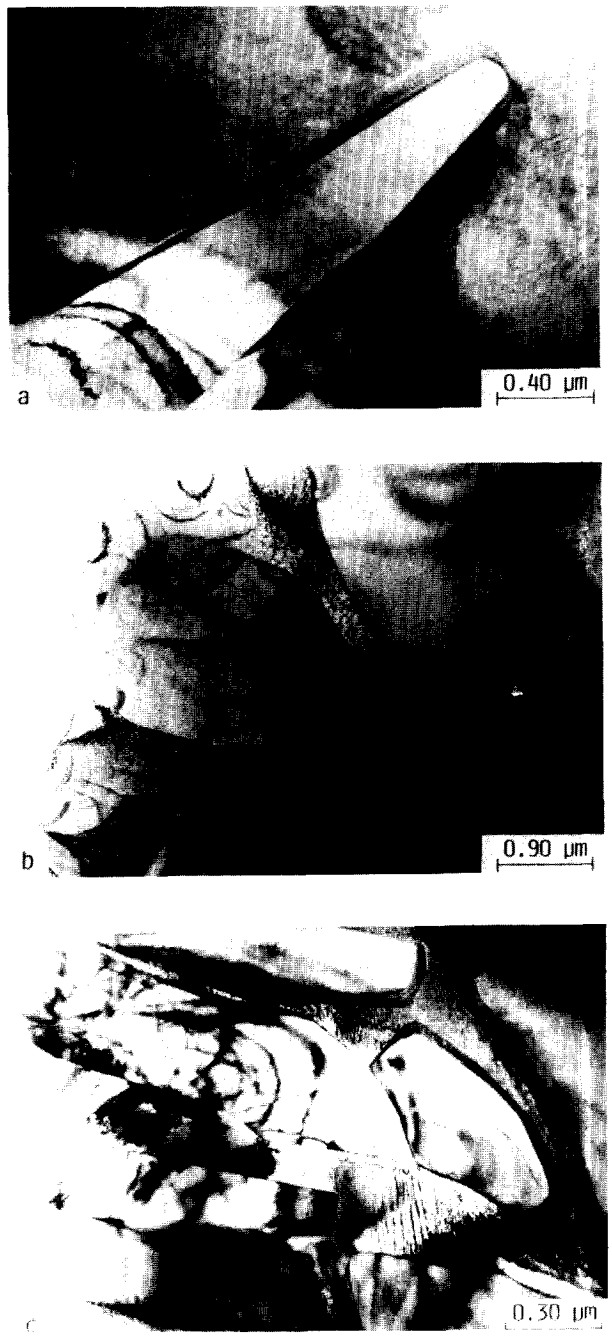

Fig. 6. (a) High-magnification and (b) low magnification bright-field transmission electron micrographs of the growth of Nb_3Al colonies from grain boundaries, in the hot-pressed and 24 h aged (1800 °C) Nb–6wt.%Al alloy during early stages of the peritectic transformation and (c) in the fully transformed condition. Note the bend contours in the grains and the high density of dislocations in the Nb_{ss} filaments.

Subsequent heat treatment at 1450 °C for 24 h resulted in the precipitation of the ordered Nb_3Al phase; the duplex structure features a uniform and fine distribution of a filamentary niobium within a non-contiguous Nb_3Al matrix (Fig. 7(b)) similar to those

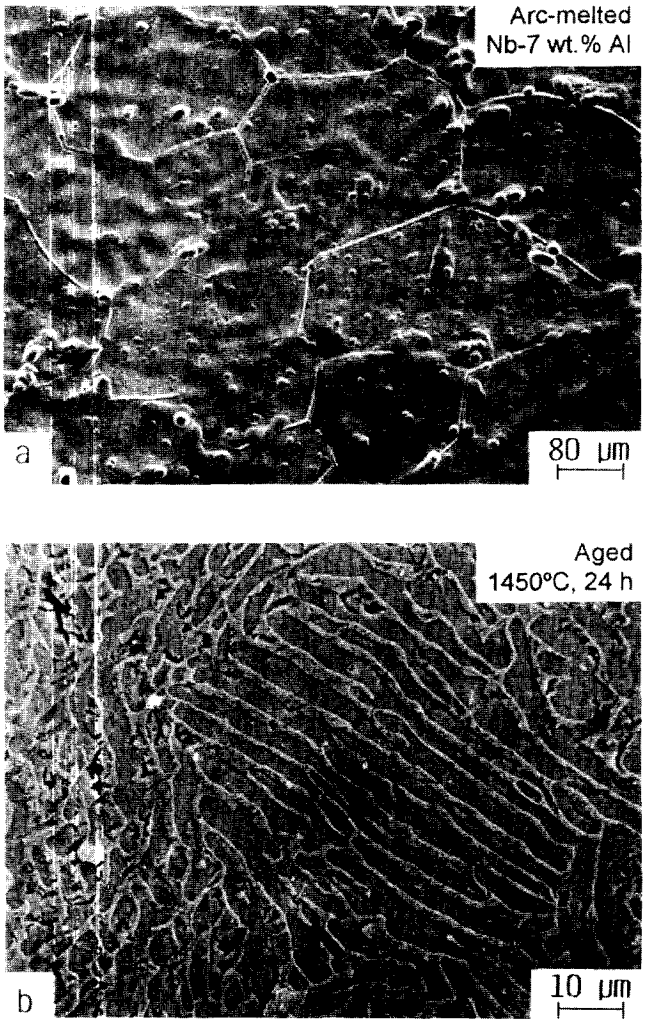

Fig. 7. Scanning electron micrographs of microstructural features of the (a) arc-melted Nb–7wt.%Al sample, showing the existence of the retained Nb_{ss} solid solution with no second phase and (b) after aging at 1400 °C for 24 h showing the lamellar Nb_{ss} + Nb_3Al solid solution microstructure.

seen above and in other studies [5, 11]. The processes involved in the development of the lamellar microstructure are also similar to those described above; the ample diffusion time assists heterogeneous nucleation of Nb_3Al colonies at grain boundaries.

3.1.4. *Unreinforced Nb_3Al*

Microstructures for monolithic Nb_3Al were relatively featureless, exhibiting a grain structure with an average size of about 50 μm. Higher magnifications reveal the presence of small Nb dendrites and some porosity (less than 2%) at certain locations in the sample; precipitation of large second-phase particles, as in the hot-pressed or thermally treated condition, was not apparent.

3.2. *Mechanical properties*

The mechanical properties of the Nb–Nb_3Al composites were distinctly superior to those of unreinforced Nb_3Al, displaying a significantly higher toughness at roughly comparable strength levels (Table 1). The unreinforced Nb_3Al material was found to have a high hardness but a very low fracture toughness ($K_{Ic} \approx 1.1$ MPa $m^{1/2}$), with an estimated yield strength (based on one third of the Vickers hardness [20]) of 274 MPa and a flexure strength of 212 MPa. In comparison, the equiaxed Nb–Nb_3Al composite showed a lower hardness but displayed a sixfold increase in toughness ($K_{Ic} \approx 6.5$ MPa $m^{1/2}$) and a flexure strength of 460 MPa, over twice that of pure Nb_3Al.

However, thermal treatments at 1800 °C lead to reductions in hardness (and strength) consistent with the fact that the microstructures are primarily hardened by the Nb_{ss} owing to the slow kinetics of Nb_3Al precipitation, especially in the 1 and 4 h aged conditions. Correspondingly, indentation toughness results suggest values in excess of 10 MPa $m^{1/2}$ (Table 1), as no cracks were observed at the corners of the indentation for loads of up to 14.5 kgf. With prolonged aging for 24 h, the Nb–6wt.%Al alloy regains its hardness concurrent with the precipitation of Nb_3Al. Although this lamellar microstructure also exhibits an increase in toughness ($K_{Ic} \approx 5.5$ MPa $m^{1/2}$), it is slightly lower than for the equiaxed microstructure; the yield and flexure strengths are also slightly reduced. Both composite microstructures display improved fatigue properties compared with monolithic Nb_3Al [21].

The fivefold to sixfold increase in toughness shown by the *in-situ* Nb–Nb_3Al composites compared with monolithic Nb_3Al can be attributed primarily to the role of ductile Nb_{ss} phase bridging of the crack, and to a lesser extent plastic deformation in the ductile phase. This is clearly evident by the presence of uncracked Nb_{ss} particles in the crack wake (Fig. 8(a) and 8(b)), which subsequently fail by ductile microvoid nucleation and growth mechanisms (Fig. 8(c)). This aspect is critical for the successful fabrication of Nb–Nb_3Al *in-situ* composites, since the ductility of Nb can be significantly degraded by contamination from interstitial impurities such as oxygen and hydrogen [22, 23].

The contribution to the toughening of Nb_3Al from the Nb_{ss} phase arises from resultant tractions bridging the two crack surfaces, thereby partially shielding the crack tip from remotely applied loads. Other mechanisms such as crack deflection, crack trapping, crack renucleation, multiple matrix cracking and decohesion along the Nb–matrix interfaces can further enhance this effect. At steady state, where the bridging zone length is at a maximum, governed by ductile ligament rupture at a critical displacement u^*, the extent of toughening due to bridging can be estimated using

TABLE 1. Mechanical properties of Nb–Nb_3Al and its unreinforced constituents

Material	Vickers hardness ($kg\,mm^{-2}$)	Rockwell hardness R_c	Estimated yield strength (MPa)	Ultimate flexure strength (MPa)	Fracture toughness K_{Ic} ($MPa\,m^{1/2}$)
Nb–Nb Al, as hot pressed (equiaxed)	661	56	220	460	6.5
Nb–Nb Al, + 1 h at 1800 °C	408	37	136	—	> 10[a]
Nb–Nb Al, + 4 h at 1800 °C	290	30	97	—	> 10[a]
Nb–Nb Al, + 24 h at 1800 °C (lamellar)	533	51	177	340	5.5
Unreinforced Nb_3Al	822	68	274	212	1.1
Unreinforced Nb	270	—	90	95	16

[a]Based on Vickers hardness indentation measurements.

simple models [4, 8] in terms of the area fraction f of ductile ligaments intersecting the crack path, their uniaxial yield strength σ_y and a representative cross-sectional radius t. These yield expressions for the composite toughness K_c of the form

$$K_c = (K_t^2 + Ef t\sigma_y \chi)^{1/2} \quad (1)$$

where K_t can be taken as the toughness of the Nb_3Al matrix. E is Young's modulus, and χ is a dimensionless representation of work of rupture [4, 8] for the specific composite. χ can vary between 0.5 and 8 depending upon the degree of interface debonding and constitutive properties of the reinforcement phase [4, 7, 8]. This formulation is applicable only under small-scale bridging conditions, where the bridging zone size is small compared with the crack length and specimen dimensions. For the equiaxed Nb–Nb_3Al composite, taking the area fraction of ductile Nb phase intercepted by the crack path as $f \approx 0.27$ (since only two thirds of the 40 vol.% Nb particles interact with the crack), yield strength for Nb $\sigma_y \approx 90$ MPa, the composite modulus $E \approx 123$ GPa, $K_t \approx 1$ $MPa\,m^{1/2}$, the Nb particle size $t \approx 5$ μm and $\chi_{Nb} \approx 2.7$ (assuming a well-bonded Nb–Nb_3Al interface [8]), the predicted composite toughness from eqn. (1) is 6.5 $MPa\,m^{1/2}$, in good agreement with the experimental result. Using similar values for the lamellar Nb–Nb_3Al composite, where $t \approx 1$ μm and $f \approx 0.4$, eqn. (1) yields a composite toughness of about 4 $MPa\,m^{1/2}$, which is somewhat lower than that observed experimentally.

4. Concluding remarks

It has been demonstrated that ductile-phase-toughened Nb–Nb_3Al intermetallic matrix composites can be successfully processed using P/M techniques, specifically by hot pressing the reaction-synthesized Nb and Al powders mixed in the ratio Nb–6wt.%Al. Utilizing the peritectic reaction in the phase diagram, the Nb morphology can be modified by thermo-mechanical treatments to fabricate a lamellar Nb–Nb_3Al composite microstructure, similar to those obtained by arc melting procedures. The P/M route is particularly advantageous over the arc-melting practice since it yields specimens with near-net shape that are readily amenable for mechanical property characterization or actual use as structural components with minimal machining.

The resulting Nb_{ss}–Nb_3Al composites show nearly a sixfold increase in fracture toughness ($K_{Ic} \approx 6$ $MPa\,m^{1/2}$), at comparable strength levels, compared with monolithic Nb_3Al ($K_{Ic} \approx 1$ $MPa\,m^{1/2}$). Such toughening is primarily attributed to crack bridging by uncracked Nb particles in the crack wake, with additional beneficial effects from plastic deformation within the Nb phase, crack deflection and renucleation, and multiple (coplanar) cracking in the matrix. Despite the marked improvement in toughness, compared with Nb_3Al, of the Nb–6wt.%Al alloy with duplex Nb–Nb_3Al microstructures, the absolute fracture toughness is still relatively low for it to be used as a structural material. Specifically, the fine micron-sized Nb particles in the present microstructures limit the formation of a significant bridging zone. In this regard, future developments toward achieving coarse microstrutures, via solid state reactions or lamination with characteristic dimensions of the Nb phase on the order of 50–500 μm, are expected to be promising.

Acknowledgments

This work was funded by the US Air Force Office of Scientific Research under Grant F49620-93-1-0107. The authors would like to thank Dr. Alan H. Rosen-

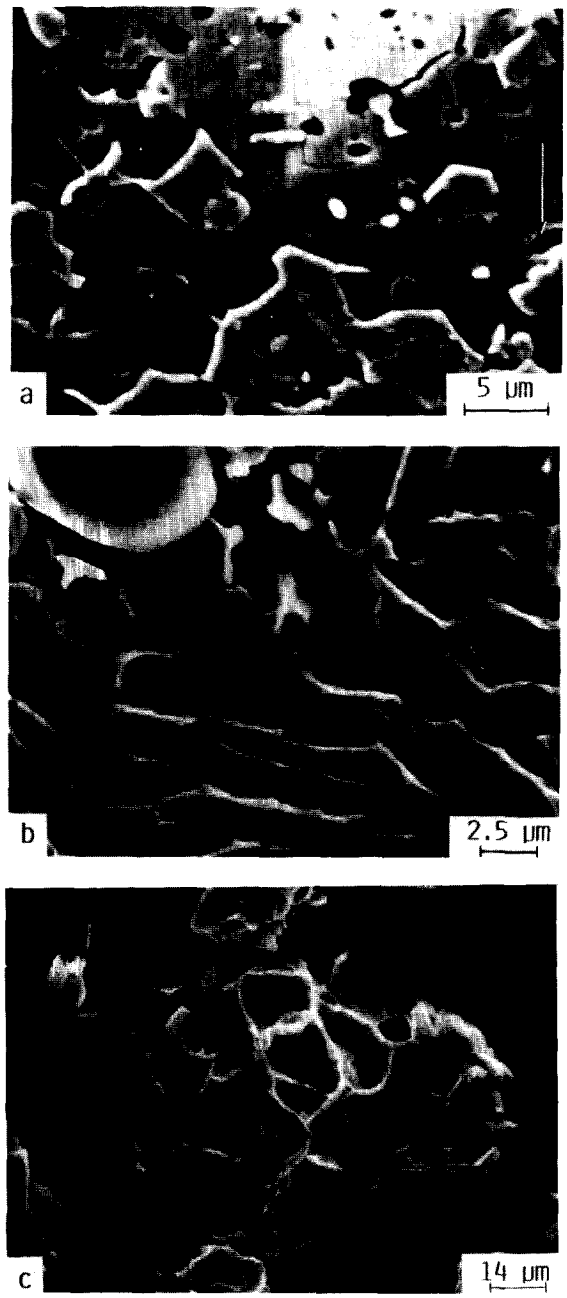

Fig. 8. Scanning electron micrographs of (a), (b) monotonic fracture paths in the (a) equiaxed and (b) lamellar Nb–Nb$_3$Al composite microstructures of the Nb–6wt.%Al alloy and (c) the corresponding fracture surface for the equiaxed structure.

stein and Dr. C. H. Ward for their support, Professor L. C. DeJonghe for helpful discussions on processing, and John Holthius, James Wu and Tyrone Mitchell for experimental assistance.

References

1 D. L. Anton and D. M. Shah, *High-Temperature Ordered Intermetallic Alloys III, Materials Research Society Symp. Proc.*, Vol. 133, Materials Research Society, Pittsburgh, PA, 1989, p. 361.
2 D. L. Anton, D. M. Shah, D. N. Duhl and A. F. Giamei, *J. Met., 41* (9) (1989) 12.
3 J. J. Stephens, *J. Met., 42* (8) (1990) 22.
4 M. F. Ashby, F. J. Blunt and M. Bannister, *Acta Metall., 37* (1989) 1847.
5 D. L. Anton and D. M. Shah, *Intermetallic Matrix Composites, Materials Research Society Symp. Proc.*, Vol. 194, Materials Research Society, Pittsburgh, PA, 1980, p. 45.
6 M. G. Mendiratta, J. J. Lewandowski and D. M. Dimiduk, *Metall. Trans. A, 22* (1991) 1573.
7 H. C. Cao, B. J. Dalgleish, H. E. Dève, C. K. Elliott, A. G. Evans, R. Mehrabian and G. R. Odette, *Acta Metall. Mater., 37* (1989) 2969.
8 H. E. Dève, A. G. Evans, G. R. Odette, R. Mehrabian, M. L. Emiliani and R. J. Hecht, *Acta Metall. Mater., 38* (1990) 1491.
9 K. T. Venkateswara Rao, G. R. Odette and R. O. Ritchie, *Acta Metall. Mater., 40* (1992) 353.
10 R. G. Rowe and D. W. Skelly, *Intermetallic Matrix Composites II Materials Research Society Symp. Proc.*, Vol. 273, Materials Research Society, Pittsburgh, PA, 1992, p. 411.
11 C. E. Lundin and A. S. Yamamoto, *Trans. Metall. Soc. AIME, 236* (1966) 863.
12 L. Kohot, R. Horyn and N. Iliev, *J. Less-Commun. Met., 44* (1976) 215.
13 L. Jorda, R. Flukinger and J. Miller, *J. Less-Commun. Met., 75* (1980) 227.
14 *ASTM Standard E399-90*, in *ASTM Standards*, Vol. 3.01, American Society for Testing and Materials, Philadelphia, PA, 1992, p. 506.
15 L. Murugesh, K. T. Kenkateswara Rao, L. C. DeJonghe and R. O. Ritchie, in K. Upadhya (ed.), *Developments in Ceramic and Metal-Matrix Composites*, Minerals, Metals and Materials Society, Warrendale, PA, 1991, p. 65.
16 C. D. Bencher, L. Murugesh, K. T. Venkateswara Rao and R. O. Ritchie, *J. Intermetall., 2* (1994) in press.
17 T. N. Marieb, A. D. Kaiser and S. R. Nutt, *High-Temperature Ordered Intermetallic Alloys IV, Materials Research Society Symp. Proc.*, Vol. 213, Materials Research Society, Pittsburgh, PA, 1991, p. 329.
18 M. Hong and J. W. Morris, Jr., *Appl. Phys. Lett., 37* (1980) 1044.
19 M. Hong, *Ph.D. Thesis*, Department of Materials Science and Mineral Engineering, University of California, Berkeley, 1980.
20 D. Tabor, *The Hardness of Metals*, Oxford University Press, Oxford, 1951.
21 L. Murugesh, K. T. Venkateswara Rao and R. O. Ritchie, *Scr. Metall. Mater., 29* (1993) 1107.
22 S. Fariabi, A. L. W. Collins and K. Salama, *Metall. Trans. A, 14* (1983) 701.
23 J. R. Donoso and R. E. Reed-Hill, *Metall. Trans. A, 7* (1976) 961.